Cerebral Cortex, May 2020;30: 3044–3054

doi: 10.1093/cercor/bhz293
Advance Access Publication Date: 14 December 2019
Original Article

ORIGINAL ARTICLE

Heritability and Cognitive Relevance of Structural Brain Controllability

Won Hee Lee[1], Amanda Rodrigue[2], David C. Glahn[2], Danielle S. Bassett[3,4,5,6,7] and Sophia Frangou[1]

[1]Department of Psychiatry, Icahn School of Medicine at Mount Sinai, New York, NY 10029, USA, [2]Tommy Fuss Center for Neuropsychiatric Disease Research, Department of Psychiatry, Boston Children's Hospital, Harvard Medical School, Boston, MA 02115, USA, [3]Department of Bioengineering, School of Engineering and Applied Science, University of Pennsylvania, Philadelphia, PA 19104, USA, [4]Department of Electrical and Systems Engineering, School of Engineering and Applied Science, University of Pennsylvania, Philadelphia, PA 19104, USA, [5]Department of Neurology, Perelman School of Medicine, University of Pennsylvania, Philadelphia, PA 19104, USA, [6]Department of Psychiatry, Perelman School of Medicine, University of Pennsylvania, Philadelphia, PA 19104, USA and [7]Department of Physics and Astronomy, College of Arts & Sciences, University of Pennsylvania, Philadelphia, PA 19104, USA

Address correspondence to Sophia Frangou, Department of Psychiatry, Icahn School of Medicine at Mount Sinai, 1425 Madison Avenue, New York, NY 10029, USA. Email: sophia.frangou@mssm.edu.

Abstract

Cognition and behavior are thought to emerge from the connections and interactions among brain regions. The precise nature of these relationships remains elusive. Here we use tools provided by network control theory to determine how the structural connectivity profile of brain regions may shape individual variation in cognition. In a cohort of healthy young adults ($n = 1066$), we computed two fundamental brain regional control patterns, average and modal controllability, which index the degree of influence of a region over others. We first established that regional brain controllability measures were both reproducible and heritable. Regions with controllability profiles theoretically conducive to facilitating multiple cognitive operations were over-represented in higher-order resting-state networks. Finally, variation in regional controllability accounted for about 50% of interindividual variability in multiple cognitive domains. We conclude that controllability is a biologically plausible property of the structural connectome and provides a mechanistic explanation for how brain structural architecture may influence cognitive functions.

Key words: cognition, controllability, diffusion magnetic resonance imaging, structural connectivity

Introduction

Among the most pressing and challenging questions in systems neuroscience, and its application to psychiatry and neurology, is how the configuration of the human brain enables the emergence of cognition and behavior. Network neuroscience models the brain as a connectome—an intricate network of brain regions that synchronize their activity via anatomical and functional connections that can be mapped and quantitatively characterized (Bassett et al. 2018; Breakspear 2017). The precise

mechanisms that underpin structure–function relationships in the brain remain the focus of intense research.

The application of graph theory has led to novel insights into the topological organization of the brain by providing new mathematical tools to model and quantify the pattern of interconnections between brain regions (Bullmore and Sporns 2009). Graph theory analyses have demonstrated that the pattern of anatomical connections of individual brain regions shows significant variation, which constitutes the main influence on the types of mental processes that can be supported (Misic and Sporns 2016; Sporns et al. 2004). These mental processes arise from continuous changes in functional brain states, which are defined as the vector of the magnitude of the neurophysiological activity across brain regions at a single time point (Gu et al. 2015; Lynn and Bassett 2019). Network control theory is an emerging multidisciplinary field of enquiry concerned with modeling how anatomical connectivity influences transitions between brain states (Betzel et al. 2016; Gu et al. 2015; Tang and Bassett 2018). The underlying assumption is that transitions in brain states are controllable, meaning that they occur along trajectories aiming to attain a target brain state chosen for its utility in meeting contextual demands (Gu et al. 2015; Lynn and Bassett 2019; Pasqualetti et al. 2014). It further posits that the anatomical connectivity of individual brain regions is critical in defining their controllability, which refers to the degree of their influence in driving transitions towards a specific target brain state (Gu et al. 2015; Lynn and Bassett 2019). The controllability of a brain region is thus linked to its structural connectivity properties which can constrain or support transitions between different brain states. The controllability of each brain region can be captured by two key metrics: average controllability (AC), which quantifies the capacity of a brain region to facilitate transitions to easy-to-reach states, and modal controllability (MC), which quantifies the ease with which a brain region can steer the brain into difficult-to-reach states (Gu et al. 2015; Lynn and Bassett 2019). The ease or difficulty of reachability of a specific brain state reflects the number of the required intervening state transitions and the inferred cost associated with these transitions (Gu et al. 2015; Pasqualetti et al. 2014). Thus, examination of patterns of regional controllability could provide an account of how the brain structural connectome may shape patterns of brain activity. However, there are yet unanswered questions regarding the controllability features of the structural connectome of the brain with regard to their consistency across large cohorts of healthy individuals, their sensitivity to genetic influence, and their association with cognitive systems and cognitive functions.

To address these knowledge gaps, we used publicly accessible high-quality neuroimaging, genetic, and cognitive data from 1066 healthy participants of the Human Connectome Project (HCP; https://www.humanconnectome.org/) to compute brain regional AC and MC. We first sought to test the interscan reliability of regional controllability in a subset of HCP participants with repeat scans and then to evaluate the heritability of controllability measures based on the HCP twin and sibling data. The structural features and functional properties of the human brain are known to be heritable (Blokland et al. 2012; Sinclair et al. 2015; Strike et al. 2018). Thus, demonstrating that regional controllability is also heritable is important for affirming its biological relevance.

Further, in assessing the cognitive relevance of regional controllability, we sought to test whether brain regions with different controllability profiles are differentially located within cognitive systems. The brain is functionally organized into cognitive systems supported by spatially defined networks (Fox et al. 2005; Power et al. 2011; Smith et al. 2009). Systems mapping to the default mode, central executive and salience networks are typically involved in diverse higher-order mental functions (Doucet et al. 2011; Menon and Uddin 2010; Raichle et al. 2001), while the auditory, visual, and sensorimotor networks support specialized sensory and motor processing (Damoiseaux et al. 2006; Smith et al. 2009). We would thus expect that regions with high AC will be preferentially located within higher-order cognitive systems where they could function to facilitate transitions to diverse states associated with these systems. Finally, we also sought to quantify the contribution of regional controllability measures to interindividual variation in higher-order cognitive functions in order to assess their relevance for cognitive task performance.

Materials and Methods

Sample

We used neuroimaging, genetic, and cognitive data from 1066 healthy participants (490 men and 576 women; age range = 22–37 years; mean age = 28.7 years) provided by the HCP (https://db.humanconnectome.org/). The outline of the work flow is shown in Figure 1. The reliability of the controllability measures was assessed using the intraclass correlation coefficient (ICC) (Shrout and Fleiss 1979) using data from 44 HCP participants (13 men and 31 women; age range = 22–35 years; mean age = 30.4 years) who had two scans with an interscan interval of 2–11 months. Supplementary analyses were also conducted by restricting the HCP sample to unrelated individuals only ($n = 339$) to address confounds related to familiality.

Construction of the Structural Connectome

Details of acquisition and preprocessing protocols for diffusion MRI (dMRI) in HCP have been provided in prior studies (Glasser et al. 2013; Sotiropoulos et al. 2013; Van Essen et al. 2012) and are also outlined in the Supplementary Material. In constructing the structural connectome, we used an in-house image processing pipeline that combines tools from DSI Studio (http://dsi-studio.labsolver.org/) and validated custom routines written in MATLAB (Mathworks) (Lee and Frangou 2017a, 2017b). The dMRI data were reconstructed in DSI Studio using generalized q-sampling imaging (GQI) (Yeh et al. 2010). GQI first reconstructs the spin distribution functions (SDFs) within each voxel and computes the quantitative anisotropy in native space. Whole-brain fiber tractography was performed using a deterministic fiber tracking algorithm that leverages information in SDFs (Yeh et al. 2013). We generated a total of 1 000 000 whole brain streamlines for each individual, with the anisotropy threshold of 0.05 and step size of 0.9 mm, determined automatically in DSI Studio. The angular threshold was 60°. Fiber tracks with lengths less than 10 mm (approximately 35 000 tracks) were discarded to prevent the tracking process from being overloaded with short association fibers.

The areal parcellation was performed by warping the standard space to the subject space using the statistical parametric mapping nonlinear registration algorithm (Ashburner and Friston 1999). We used a template derived from the automated anatomical labeling template (Tzourio-Mazoyer et al. 2002) that subdivides the brain into 512 cortical and subcortical regions with approximately uniform volume as previously described (Zalesky et al. 2010) (Supplementary Table S1). For each partici-

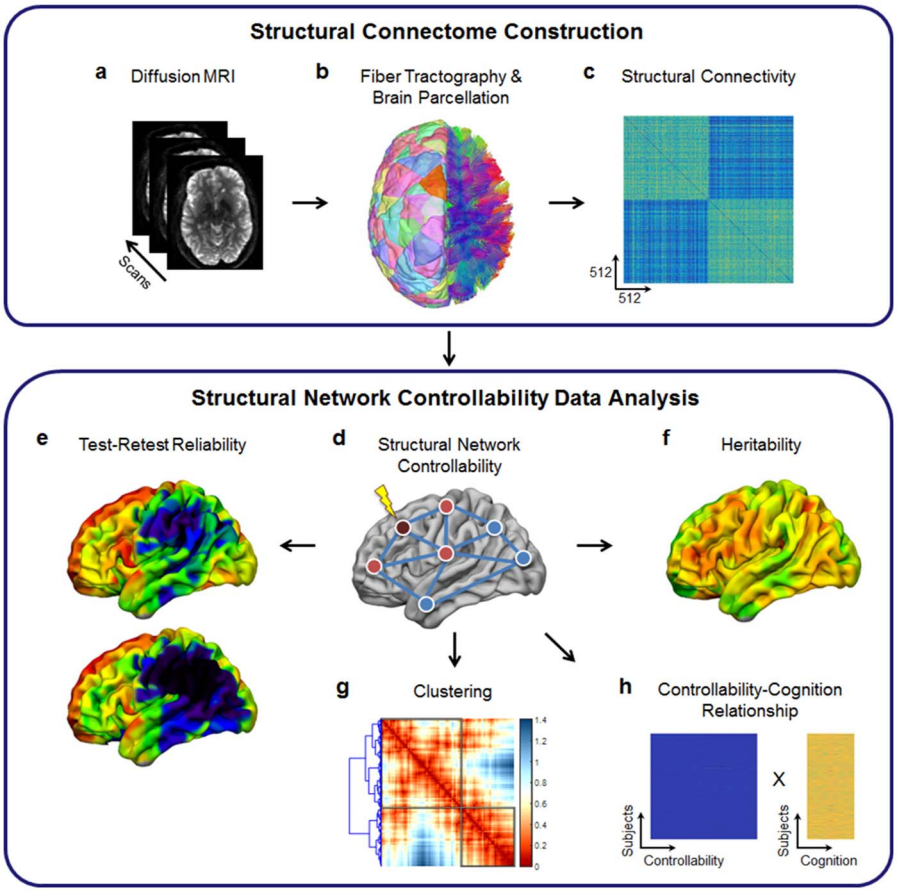

Figure 1. Overview of the workflow. (*a*) We analyzed diffusion magnetic resonance imaging data obtained from 1066 healthy participants of the HCP. (*b*) Fiber tractography was performed in each participant. The structural connectome was characterized using a parcellation of 512 brain regions. (*c*) A weighted structural connectivity matrix of size 512×512 was constructed representing the streamline counts between pairs of regions. (*d*) Average (AC) and modal controllability (MC) at each brain region were computed for each participant. (*e*) Test–retest reliability of regional AC and MC in a dataset of 44 HCP participants that had repeat scans was assessed using the ICC. (*f*) The heritability of regional AC and MC was computed. (*g*) Brain regions were clustered based on AC and MC measures. (*h*) Multivariate PLSs was used to quantify the association between measures of regional controllability and multidomain cognitive measures.

pant, we generated a weighted, undirected structural connectivity matrix, A, each element of which, A_{ij}, represents the number of streamlines connecting any pair of regions i and j. We did not binarize the structural connectivity matrix, A, since many real-world networks, including human brain networks (Bassett and Bullmore 2016), are better characterized by weighted graphs, in which brain regions are represented by network nodes, and their structural connections by weighted edges (Bassett et al. 2018).

Computation of Regional Average and Modal Controllability

The procedures for computing regional controllability measures have been previously detailed and are derived from established mathematical formulations (Gu et al. 2015; Tang et al. 2017; Wu-Yan et al. 2018). Specifically, the brain is represented as a network of n nodes governed by the following noise-free, linear, discrete-time, and time-invariant dynamics (Galan 2008; Honey et al. 2009; Pasqualetti et al. 2014):

$$x(t+1) = Ax(t) + Bu(t), \tag{1}$$

where $x(t) = \{x_1(t), \ldots, x_n(t)\}$ denotes the state of nodes at time t. The term A denotes a symmetric, weighted structural connectivity matrix (of size $n \times n$) in which element A_{ij} represents the number of white matter streamlines connecting nodes i and j. The diagonal elements of A are set to zero ($A_{ii} = 0$). To ensure Schur stability, the matrix is divided by $1 + \xi_0(A)$, where $\xi_0(A)$ is the largest singular value of A. The term $u(t) = \{u_1(t), \ldots, u_p(t)\}$ is referred to as the control energy and denotes a vector collecting the p external inputs applied to the set of control nodes indicated in B at time t. The input matrix B specifies the control node(s) in the network, whose entry B_{ij} is one, if the input $u_j(t)$ affects the state $x_i(t)$, otherwise it is zero. According to the classic Kalman rank condition (Chen 1999; Kalman 1963), the system described by equation (1) is controllable if and only if

$$\text{rank}(C) = \text{rank}\left(\left[B\ AB\ A^2B \ldots A^{n-1}B\right]\right) = n, \tag{2}$$

where $C = \left[B\ AB\ A^2B \ldots A^{n-1}B\right]$ is called the controllability matrix (of size $n \times np$) and has full row rank n. The controllability of a network can be equivalently characterized by means of the discrete controllability Gramian W, defined by

$$W = \sum_{\tau=0}^{\infty} A^{\tau} B B^{T} \left(A^{T}\right)^{\tau}, \tag{3}$$

where T denotes the transpose operation and τ indicates the time step of the trajectory. The system is controllable if and

only if W is positive definite or equivalently if the minimum eigenvalue of W is strictly larger than zero (Chen 1999). We chose to control nodes one at a time, and thus the input matrix B in fact reduces to a one-dimensional vector, for example, $B_{ij} = (1\ 0\ 0 \ldots)^T$ when the first brain region is the control node. In general, the ease or difficulty of control is related to the structure and eigenvalues of the controllability Gramian (Wu-Yan et al. 2018). Based on this theoretical foundation, the AC is computed as the trace of the controllability Gramian matrix W_k,

$$\zeta = \text{Trace}\,(W_k)\,, \tag{4}$$

where W_k is the Gramian calculated from the node k and MC is computed from the eigenvector matrix $V = [v_{ij}]$ of the network adjacency matrix A, defined by

$$\phi_i = \sum_j \left(1 - \xi_j^2\,(A)\right) v_{ij}^2, \tag{5}$$

as a scaled measure of the controllability of all N modes $\xi_1\,(A)$, $\ldots$, $\xi_{N-1}\,(A)$ from brain region i.

We followed the procedures outlined above to compute the AC and MC for each of the 512 brain regions in each participant. Further, we confirmed the validity of these results (Supplementary Fig. S1), by comparing findings from the empirical data to those obtained from null network models constructed by randomly permuting the connection (edge) weights of the connectivity matrix using either a strength- or degree-preserving randomization scheme implemented in the Brain Connectivity Toolbox (Rubinov and Sporns 2010).

Assessment of Heritability of Regional Controllability

Heritability estimates were calculated using Sequential Oligogenic Linkage Analysis Routines software (Almasy and Blangero 1998), which employs maximum likelihood variance decomposition methods to determine the relative importance of genetic and environmental influences by modeling the covariance among family members as a function of genetic proximity. Age, age^2, sex, and their interactions (age $\times$ sex, age^2 $\times$ sex) were tested as covariates of interest by comparing the likelihood of a model estimating the covariate effect to the likelihood of a model where the covariate effect was constrained to zero. See Supplementary Material for more details.

Regional Controllability Profiles and Cognitive Systems

In order to evaluate the potential functional consequences of the brain regional controllability, we tested whether regions that differed in their controllability profile were differentially located within known cognitive systems mapped to spatially defined networks. Here, we focused on six large-scale networks, namely the auditory (AUD), central executive (CEN), default mode (DMN), salience (SAL), somatosensory (SMN), and visual (VIS) networks which we defined using the template provided by Power and colleagues (Power et al. 2011), which was originally derived from the resting-state functional MRI data. We refer to these networks as cognitive systems based on prior research which established that the functional architecture of the brain at rest corresponds to the functional networks mapped to cognitive domains in activation studies (Cole et al. 2014; Smith et al. 2009). We assigned each of the 512 brain regions to a single network based on the closest Euclidian distance between each region and the Power parcellation template (Supplementary Table S2).

To identify clusters of regions with different controllability profiles, we used data-driven hierarchical clustering using Ward's minimum variance method (Ward 1963) for Euclidean distances between pairs of ranked controllability measures. The optimal cluster number was determined using the Davies–Bouldin (DB) index, which is the ratio of intracluster similarity to intercluster differences for a given clustering solution (Davies and Bouldin 1979). Lower DB index values indicate a better clustering solution. We then computed the percentage of brain regions in each cluster present from each of the six cognitive systems. To correct for system size, we normalized the raw percentage of brain regions located in a given cognitive system by the total number of regions in a cognitive system. To confirm the reproducibility of the findings, we repeated the analyses using an alternative functional template provided by Yeo and colleagues (Yeo et al. 2011).

Regional Controllability and Cognitive Function

We considered nine cognitive variables from the HCP database that cover all aspects of cognition: crystallized cognition (NIMH Toolbox Crystallized Cognition Composite), fluid intelligence (Penn Matrix Test: Number of Correct Responses), working memory (List Sorting Working Memory Test), sustained attention (Short Penn Continuous Performance Test Sensitivity and Specificity), language comprehension (Picture Vocabulary Test), cognitive flexibility (Dimensional Change Card Sort Scale Score), inhibitory control (Flanker Inhibitory Control and Attention Test), and emotion recognition (Penn Emotion Recognition: Number of Correct Responses) (Supplementary Table S3).

We applied multivariate partial least squares (PLSs) to model the associations between the cognitive variables detailed above and regional average and MC (Krishnan et al. 2011; McIntosh and Lobaugh 2004). PLS models the associations between two sets of variables by means of latent variables (LVs) and was chosen because it is a data-driven approach that has been successfully used to identify associations between cognitive and neuroimaging measures (Krishnan et al. 2011). The two main advantages of PLS are its sensitivity in detecting subtle and spatially distributed brain-cognition associations and its explicit modeling of the effects of variables that are collinear or near-linear, which is often the case with cognitive and brain imaging measures.

The associations between cognition and AC or MC were examined in two separate PLS analyses controlling for age and sex or age^2 and sex. The total brain volume was also entered as a covariate in all models as it showed univariate correlations with controllability measures at a nominal uncorrected significance level. We created two controllability matrices: one for regional AC and the other for regional MC (each controllability matrix: size of 1066×512, representing, respectively, the number of participants and the number of regions). We also constructed a matrix for the cognitive data (cognitive matrix: size of 1066×9, representing, respectively, the number of participants and the number of cognitive variables included). The controllability and cognitive data were z-scored across subjects prior to performing the PLS analyses. We proceeded to compute the covariance matrix between the controllability and cognitive matrices, and then we decomposed the resulting covariance matrix into sets of

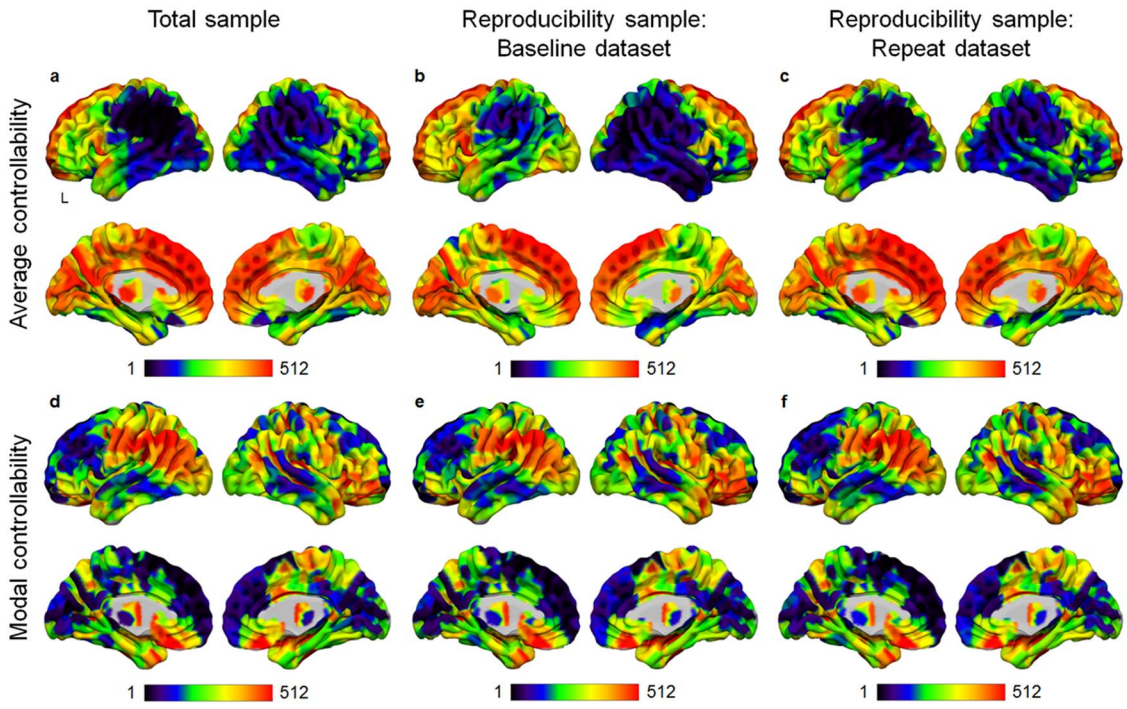

Figure 2. Regional average (AC) and modal controllability (MC). The ranked mean value of the AC of each of the 512 brain regions in the (*a*) entire sample ($n = 1066$) and in the (*b*) baseline and (*c*) repeat scans of a reproducibility subsample ($n = 44$). The ranked mean value of the MC of each of the 512 brain regions in the (*d*) entire sample ($n = 1066$) and in the (*e*) baseline and (*f*) repeat scans of a reproducibility subsample ($n = 44$). The ranked controllability values are projected onto the cortical surface for ease of visualization. L: Left. Additional information is provided in Supplementary Figure S2 and Tables S4 and S5.

orthogonal LVs. Permutation testing and bootstrap resampling were used to determine statistical significance for controllability patterns and for the contribution of individual nodes to these patterns, respectively. The significance of LVs was assessed using permutation tests (1000 iterations) of the singular values from singular value decomposition of controllability and cognitive matrices. The reliability of each controllability estimate to the LV was assessed using bootstrap resampling (3000 iterations). Bootstrapping also allowed us to estimate a bootstrap ratio for each brain region, which is the ratio of the weight of regional controllability over its estimated standard error, where each ratio approximates a z-score for the contribution of the controllability of each region to the association of interest (Zimmermann et al. 2018). A high, positive bootstrap ratio indicates that the corresponding region contributes positively and reliably to the controllability–cognition relationship identified by the LV correlation. In contrast, a high, negative bootstrap ratio means that the corresponding region contributes negatively and reliably to the controllability–cognitive relationship. For each LV, we reported results with an absolute bootstrap ratio above 3, which corresponds to robustness at a confidence level of approximately 99% (Garrett et al. 2013)

Results

Regional Average and Modal Controllability

Fig. 2*a*,*d*, respectively, show the AC and MC for each of the 512 regions averaged across 1066 participants (additional details in Supplementary Fig. S2 and Tables S4 and S5). AC was highest bilaterally in the medial prefrontal and anterior cingulate gyri, the supplementary motor area, and the precuneus. MC was highest bilaterally in the orbital prefrontal gyrus, the somatosensory cortex, the supramarginal gyrus, the insula, the medial temporal gyrus, and the thalamus. The results remained the same when the analyses were restricted only to unrelated study participants (Supplementary Fig. S3).

Reproducibility of Regional Controllability

Figure 2*b*-*c*,*e*-*f*, respectively, show the within-subject ICC of the AC and MC for each of the 512 regions averaged across 44 HCP participants with two scanning sessions. The mean ICC for regional AC and MC was, respectively, 0.71 ± 0.15 and 0.77 ± 0.09 (Supplementary Fig. 4). The ICC for AC was highest in the middle and inferior occipital gyri, the superior parietal gyrus, the precuneus, and the middle temporal gyrus (additional details in Supplementary Tables S6 and S7), and the ICC for MC was highest in the precuneus, the supplementary motor area, the inferior and middle temporal gyri, the fusiform gyrus, and the inferior parietal gyrus (additional details in Supplementary Tables S6 and S7).

Heritability of Regional Average and MC

Heritability estimates of AC and MC were generally high in multiple cortical and subcortical regions (Fig. 3 and Supplementary Fig. S5). The thalamus, striatal regions, and ventral prefrontal regions had the highest values, while the lowest values were noted in the medial superior frontal gyrus, the paracentral lobule, the middle frontal gyrus, the postcentral gyrus, and the supramarginal gyrus (additional details in Supplementary Tables S8 and S9).

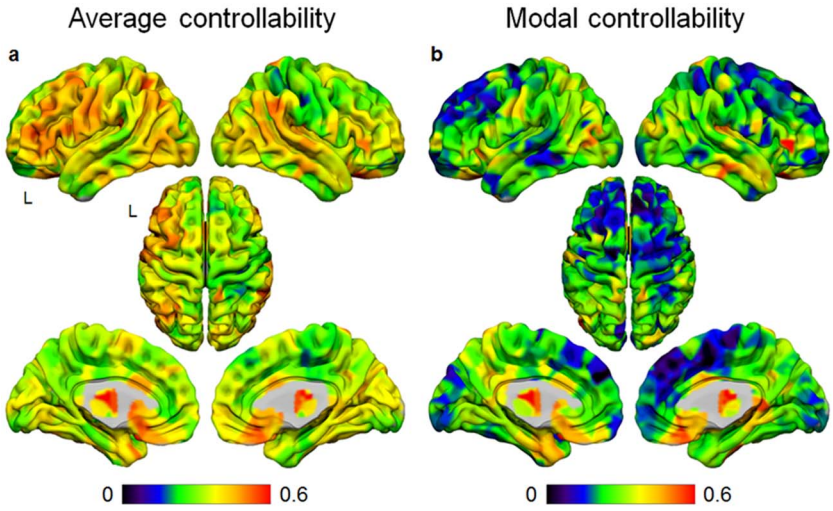

Figure 3. Heritability of structural brain controllability. Heritability of (*a*) Average Controllability and (*b*) Modal Controllability for each of the 512 brain regions. L: Left. Additional details are provided in Supplementary Figure S5 and Tables S8 and S9.

Regional Controllability Profiles and Cognitive Systems

Hierarchical clustering (Fig. 4*a–d*) identified two clusters of brain regions: cluster 1 including regions with high AC and low MC and cluster 2 comprising regions with low AC and high MC. As shown in Figure 4*e*, regions with high AC/low MC were over-represented in higher-order networks (DMN, CEN), while regions with low AC/high MC were over-represented in lower-order networks (AUD, SMN) ($\chi^2 = 41.1$, $P < 0.001$). These findings remained consistent when an alternative functional parcellation atlas was used to define the cognitive systems (Supplementary Fig. S6).

Regional Controllability and Cognitive Function

The PLS model obtained for AC yielded two LVs, LV1 ($P = 0.001$, 50%) and LV2 ($P = 0.001$, 19%), which showed significant contributions to the covariance (Fig. 5*a–d* and Supplementary Fig. S7). The dominant LV1 exhibited positive weightings from all of the cognitive variables (Fig. 5*a*). The corresponding AC profile emphasized positive contributions primarily for the precuneus and posterior cingulate gyrus and negative contributions for the postcentral and supplementary motor area, the middle frontal, and inferior parietal gyri (Fig. 5*b*; Supplementary Table S10). The pattern for LV2 revealed smaller and more mixed associations with the cognitive variables: the scores for crystalized cognition and language comprehension showed negative weighting, while the scores for cognitive flexibility, inhibitory control, sustained attention, and emotion recognition showed positive weightings (Fig. 5*d*). The corresponding AC profile highlighted positive correlations from the anterior and middle anterior cingulate gyri and negative contributions primarily from regions in the motor and somatosensory cortex and the visual stream (Fig. 5*d*; Supplementary Table S10). The results remained the same when analyses were restricted only to unrelated HCP participants (Supplementary Fig. S8).

The PLS model obtained for MC yielded two LVs, LV1 ($P = 0.001$, 48%) and LV2 ($P = 0.012$, 15%), which showed significant contributions to the covariance (Fig. 5*e–h* and Supplementary Fig. S7). The correlations of the cognitive variables with LV1 (Fig. 5*e*) and LV2 (Fig. 5*g*) were the mirror image of those observed for the respective LVs in the PLS for AC (Supplementary Table S11). For the corresponding MC profile, the pattern of correlations with LV1 (Fig. 5*f*) and LV2 (Fig. 5*h*) identified similar brain regions to those observed for the respective LVs in the PLS for AC (Supplementary Table S11). The results remained the same when analyses were restricted only to unrelated HCP participants (Supplementary Fig. S8).

Discussion

The present study leveraged the data of the HCP to test the heritability and cognitive relevance of two regional metrics, AC and MC, that quantify the influence individual brain regions might be expected to have in facilitating or constraining transitions between brain states based on their anatomical connectivity. We demonstrated that the AC and MC of brain regions are reliable and heritable properties of the human structural connectome and are related to multidomain cognitive task performance. We therefore argue that structural controllability measures provide a robust and biologically plausible mechanism for how the human brain structural organization may shape individual differences in brain function.

Reliability and Reproducibility of Brain Regional Controllability

The application of a range of neuroimaging analyses has increased the potential to yield novel metrics aiming to describe the organizational properties of the brain. The reliability and reproducibility of such measures are particularly important when considering their biological plausibility and usefulness. In this study, we showed high test-retest reliability of the AC and MC in a subsample of participants with repeat scans. Our results reinforce prior studies which found that the spatial distribution of AC and MC shows remarkable consistency across independent cohorts, MR acquisition parameters, and brain parcellation methods (Cornblath et al. 2019; Gu et al. 2015; Jeganathan et al. 2018). Across studies, the regions with the highest AC reliably include the precuneus/posterior cingulate gyrus, and the medial prefrontal/anterior cingulate cortex (Cornblath et al. 2019; Gu et al. 2015; Jeganathan et al. 2018). We

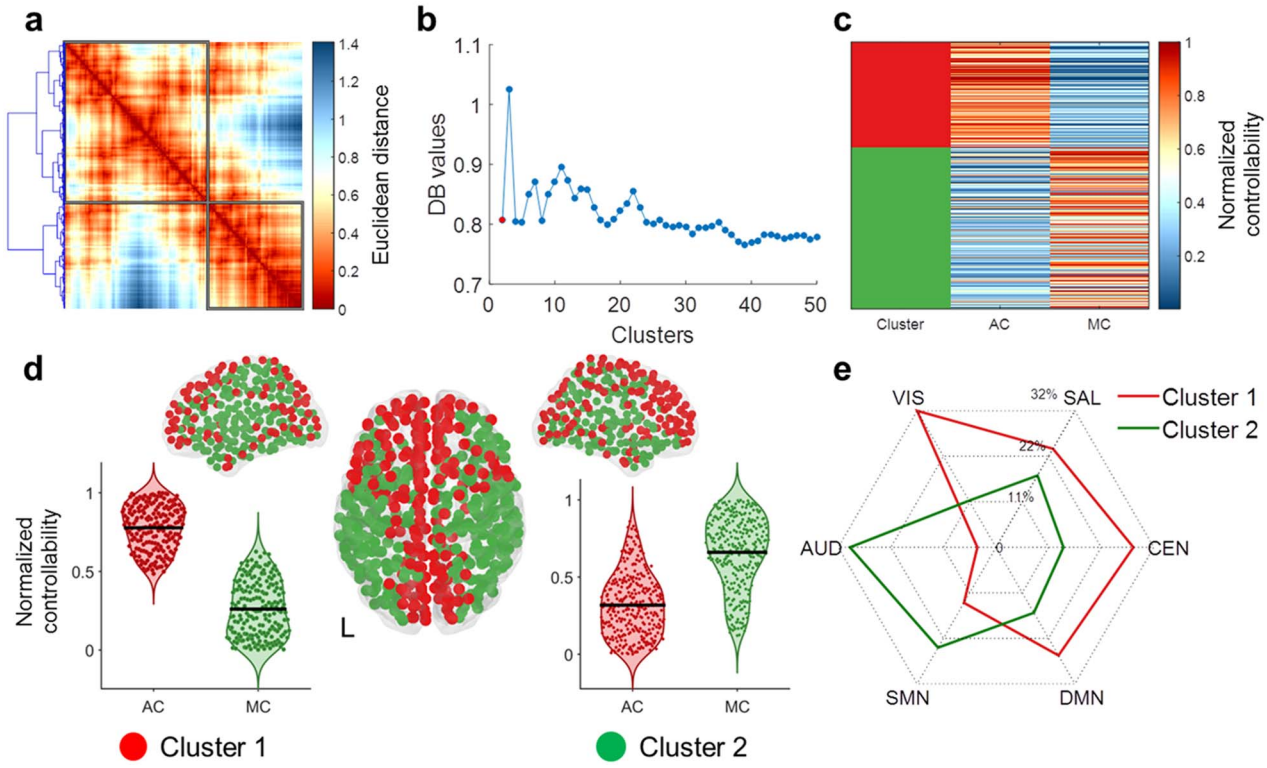

Figure 4. Regional controllability profiles and cognitive systems. (*a*) Dendrogram resulting from hierarchical clustering of 512 brain regions based on their AC and MC. (*b*) A two-cluster solution was supported by the DB criterion. (*c*) Matrix of the controllability measures for the two-cluster solution (red and green). Each row is a brain region and each column is a measure. (*d*) Violin plots of nodal AC and MC of the two different clusters. (*e*) Radar plots showing the percentage of brain regions in each cluster localized in the cognitive systems. AUD, auditory network; CEN, central executive network; DMN, default mode network; SAL, salience network; SMN, somatosensory network; VIS, visual network. L: Left.

note that these regions correspond to densely connected hubs that form the core of the structural connectome (Hagmann et al. 2008). Similar interstudy reproducibility is noted for regions showing high MC that consistently include the postcentral, supramarginal, inferior parietal, and orbital and rostromedial prefrontal regions, considered as nonhubs of the structural connectome (Hagmann et al. 2008).

AC and MC Are Heritable

AC and MC showed substantial and largely bilaterally symmetric heritability for most brain regions, thus affirming their biological relevance and supporting future investigations into their molecular genetic correlates. The range of heritability estimates for both types of controllability was generally higher for subcortical regions and especially for the thalamus (range: 0.32–0.67) and the putamen (range: 0.21–0.60), followed by prefrontal regions for AC (range: 0.16–0.52) and posterior and sensory regions (range: 0.04–0.51) for MC. These findings are aligned with the range of values reported for other brain phenotypes. In the HCP dataset, twin-based heritability estimates of cortical thickness have been shown to range from nearly 0% for orbitofrontal regions to 64% for the left superior frontal gyrus, the left superior parietal cortex, and the right postcentral gyrus (Strike et al. 2018). In a separate meta-analysis of twin studies (Blokland et al. 2012), the heritability estimates were generally higher for subcortical volumes than for regional cortical thickness, with the highest estimates (range: 78.4–81.6%) noted for the putamen. The heritability estimates of controllability were also comparable with those reported for brain topological properties such as global efficiency (range: 0.52–0.64), clustering coefficient (range: 0.47–0.59), and small-worldness (range: 0.51–0.59) (Sinclair et al. 2015). These findings implicate genes or genetic factors that influence variation in structural connectivity across multiple rather than discrete brain regions. This argument is similar to findings regarding the genetic architecture of general intelligence versus that of discrete cognitive domains (Bearden and Glahn 2017).

Regional Brain Controllability and Cognitive Systems

Using data-driven approach, we distinguished between a cluster of regions with high AC/low MC and a cluster of regions with low AC/high MC (Fig. 4). We hypothesized that regions with high AC are likely to be control nodes in high-order systems where they are theoretically expected to play a crucial role in "easing" transitions to the multiple brain states linked with these systems. In line with this prediction, we note that two known "flexible hubs" (Anderson et al. 2013; Cole et al. 2013; Crossley et al. 2013; van den Heuvel and Sporns 2013), namely the medial prefrontal/anterior cingulate cortex and precuneus/posterior cingulate cortex, were assigned to the cluster characterized by a high AC/low MC profile. Other regions with high AC/low MC were also relatively over-represented in higher-order systems and particularly the DMN and CEN. This is consistent with prior evidence that these systems include a

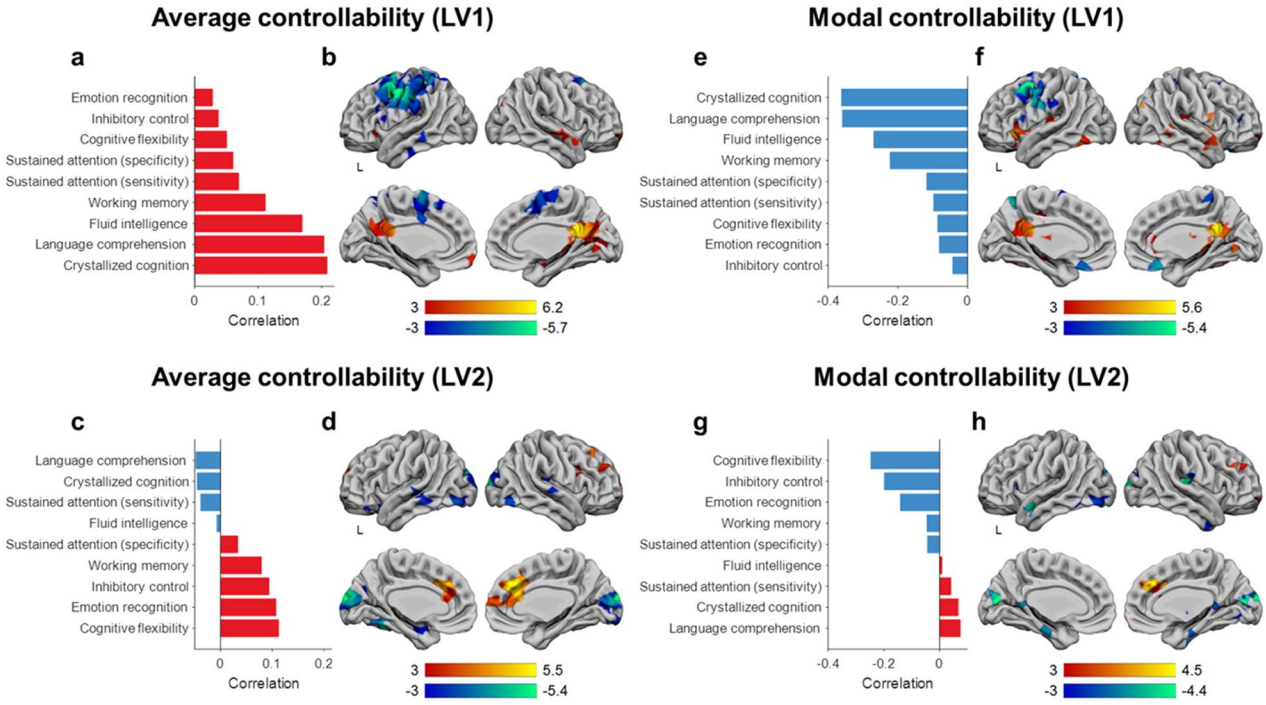

Figure 5. Regional controllability and cognitive function. AC (panels *a*–*d*): The PLSs model identified two significant LVs LV1 and LV2 which, respectively, accounts for 50% and 19% of the covariance between AC and cognition. For each LV, (panels *a* and *c*) we show the correlations between AC scores and cognitive variables and (panels *b* and *d*) we map the bootstrap ratios of the weights of AC of the corresponding regions. MC (panels *e*–*h*): The PLS model for MC identified two significant LVs LV1 and LV2 which, respectively, account for 48% and 15% of covariance between MC and cognition. For each LV, (panels *e* and *g*) we show the correlations between MC scores and cognitive variables and (panels *f* and *e*) we map the bootstrap ratios of the weights of MC of the corresponding regions. In all models, a region with positive bootstrap ratio contributes positively to the controllability-cognition covariation, while a region with a negative bootstrap ratio contributes negatively to the controllability-cognition covariation. Bootstrap ratios for all LVs were thresholded at bootstrap ratios$| > 3$, $P < 0.01$. The names of the cognitive variables as coded in the HCP database are provided in Supplementary Table S3. L: left.

higher percentage of "flexible" brain regions whose functional connectivity patterns can be rapidly updated to meet contextual demands (Anderson et al. 2013; Cole et al. 2013; Crossley et al. 2013; van den Heuvel and Sporns 2013). By contrast, brain regions with low AC/high MC were over-represented in the low-order sensory and motor systems (Fig. 4*e*). Regions within these systems mostly have dense local connections consistent with their known involvement in local, rather than wide-ranging and circumscribed functions. Our findings suggest that a subset of these regions has a high MC/low AC profile and thus theoretically important in enabling these localized systems to influence transitions to brain states beyond the boundaries of their specialized functions.

Regional Brain Controllability and Individual Variation in Cognition

The importance of regional AC and MC for individual variation in cognitive task performance can be deduced from the pattern of associations with cognition modeled by the dominant LVs (LV1) in the PLS analyses for AC and MC. The PLS models for AC and MC revealed, respectively, positive and negative associations with individual variation in task performance across multiple cognitive domains. Both PLS models reinforced the positive contribution of regions with high AC/low MC to individual difference in cognition.

In both PLS analyses, the second LV (LV2) revealed a mixed pattern of positive and negative weightings indicative of a dissociation between tests that map to specific, goal-directed functions (working memory, inhibitory control, and cognitive flexibility) (Stuss and Alexander 2000) and those that index more global processes (composite crystalized cognition and language comprehension). Of note, the pattern of correlations for emotion recognition in the LV2 in both PLS analyses followed that for executive functions; this is consistent with recent meta-analyses that show convergence between the superordinal networks for executive function and affect processing, particularly in the anterior cingulate cortex and portions of the visual cortex (Fusar-Poli et al. 2009; Lindquist et al. 2016; Niendam et al. 2012).

Methodological Considerations

It is also important to acknowledge several methodological limitations that could be addressed in future studies. Structural connectivity in this study was estimated from dMRI data and associated tractography algorithms using current standard methods for mapping the structural connections of the human brain (Stiso et al. 2018; Tang et al. 2017). This approach may undersample long-range white matter tracts, particularly in regions where fibers are densely populated, and show sharp directional changes (Thomas et al. 2014). Emerging imaging techniques such as diffusion spectrum imaging may improve estimates of structural network architecture in future studies (Baum et al. 2018; Betzel et al. 2016; Betzel et al. 2017; Gu et al. 2015; Pestilli et al. 2014; Roalf et al. 2016). Evidence from

this and previous studies suggests that average and MC may increase during childhood and adolescence (Cornblath et al. 2019) and reaches a plateau in young adulthood. Larger studies with more comprehensive coverage of the human lifespan are needed to provide a definitive age-related trajectory of regional controllability and its association with cognition. Future studies involving functional MRI data will be important in elucidating more precisely how different aspects of controllability contribute to functional brain states and cognition.

In summary, we provide evidence that controllability that models the dynamic properties of the brain as inferred from the structural connectome is a biologically plausible metric that has the potential to provide mechanistic insights into the relationship between cognitive functions and the structural organization of the human brain.

Supplementary Material

Supplementary material is available at *Cerebral Cortex* online.

Funding

National Institute of Mental Health (grant R01MH113619); the John D. and Catherine T. MacArthur Foundation; the Alfred P. Sloan Foundation; the ISI Foundation; the Paul Allen Foundation; the Army Research Laboratory (W911NF-10-2-0022); the Army Research Office (Bassett-W911NF-14-1-0679, Grafton-W911NF-16-1-0474, DCIST-W911NF-17-2-0181); the Office of Naval Research; the National Institute of Mental Health (2-R01-DC-009209-11, R01-MH112847, R01-MH107235, R21-M MH-106799, R01-M MH-113550); the National Institute of Neurological Disorders and Stroke (R01 NS099348); the National Institute of Child Health and Human Development (1R01HD086888-01); the National Science Foundation (BCS-1441502, BCS-1430087, NSF PHY-1554488, BCS-1631550) to D.S.B. Data were provided by the Human Connectome Project (HCP), and the Washington University, University of Minnesota, and Oxford University Consortium (Principal Investigators David Van Essen and Kamil Ugurbil; Grant 1U54MH091657) funded by 16 National Institutes of Health and Centers that support the NIH Blueprint for Neuroscience Research, and the McDonnell Center for Systems Neuroscience at Washington University.

Notes

The content is solely the responsibility of the authors and does not necessarily represent the official views of any of the funding agencies. The authors declare no competing financial interests. *Conflict of Interests*: None declared.

References

Almasy L, Blangero J. 1998. Multipoint quantitative-trait linkage analysis in general pedigrees. *Am J Hum Genet*. 62(5):1198–1211.

Anderson ML, Kinnison J, Pessoa L. 2013. Describing functional diversity of brain regions and brain networks. *NeuroImage*. 73:50–58.

Ashburner J, Friston KJ. 1999. Nonlinear spatial normalization using basis functions. *Hum Brain Mapp*. 7(4):254–266.

Bassett DS, Bullmore ET. 2016. Small-world brain networks revisited. *Neuroscientist*.

Bassett DS, Zurn P, Gold JI. 2018. On the nature and use of models in network neuroscience. *Nat Rev Neurosci*. 19(9):566–578.

Baum GL, Roalf DR, Cook PA, Ciric R, Rosen AFG, Xia C, Elliott MA, Ruparel K, Verma R, Tunc B, et al. 2018. The impact of in-scanner head motion on structural connectivity derived from diffusion mri. *NeuroImage*. 173:275–286.

Bearden CE, Glahn DC. 2017. Cognitive genomics: searching for the genetic roots of neuropsychological functioning. *Neuropsychology*. 31(8):1003–1019.

Betzel RF, Gu S, Medaglia JD, Pasqualetti F, Bassett DS. 2016. Optimally controlling the human connectome: the role of network topology. *Sci Rep*. 6:30770.

Betzel RF, Medaglia JD, Kahn AE, Soffer J, Schonhaut DR, Bassett DS. 2017. Inter-regional ecog correlations predicted by communication dynamics, geometry, and correlated gene expression. *ArXiv e-prints*. https://ui.adsabs.harvard.edu/#abs/2017arXiv170606088B (last accessed 1 June 2017).

Blokland GA, de Zubicaray GI, McMahon KL, Wright MJ. 2012. Genetic and environmental influences on neuroimaging phenotypes: a meta-analytical perspective on twin imaging studies. *Twin Res Hum Genet*. 15(3):351–371.

Breakspear M. 2017. Dynamic models of large-scale brain activity. *Nat Neurosci*. 20(3):340–352.

Bullmore E, Sporns O. 2009. Complex brain networks: graph theoretical analysis of structural and functional systems. *Nat Rev Neurosci*. 10(3):186–198.

Chen C-T. 1999. *Linear system theory and design*. New York: Oxford University Press.

Cole MW, Bassett DS, Power JD, Braver TS, Petersen SE. 2014. Intrinsic and task-evoked network architectures of the human brain. *Neuron*. 83(1):238–251.

Cole MW, Reynolds JR, Power JD, Repovs G, Anticevic A, Braver TS. 2013. Multi-task connectivity reveals flexible hubs for adaptive task control. *Nat Neurosci*. 16(9):1348–1355.

Cornblath EJ, Tang E, Baum GL, Moore TM, Adebimpe A, Roalf DR, Gur RC, Gur RE, Pasqualetti F, Satterthwaite TD, et al. 2019. Sex differences in network controllability as a predictor of executive function in youth. *NeuroImage*. 188:122–134.

Crossley NA, Mechelli A, Vertes PE, Winton-Brown TT, Patel AX, Ginestet CE, McGuire P, Bullmore ET. 2013. Cognitive relevance of the community structure of the human brain functional coactivation network. *Proc Natl Acad Sci U S A*. 110(28):11583–11588.

Damoiseaux JS, Rombouts SA, Barkhof F, Scheltens P, Stam CJ, Smith SM, Beckmann CF. 2006. Consistent resting-state networks across healthy subjects. *Proc Natl Acad Sci U S A*. 103(37):13848–13853.

Davies DL, Bouldin DW. 1979. A cluster separation measure. *IEEE Trans Pattern Anal Mach Intell*. 1(2):224–227.

Doucet G, Naveau M, Petit L, Delcroix N, Zago L, Crivello F, Jobard G, Tzourio-Mazoyer N, Mazoyer B, Mellet E, et al. 2011. Brain activity at rest: a multiscale hierarchical functional organization. *J Neurophysiol*. 105(6):2753–2763.

Fox MD, Snyder AZ, Vincent JL, Corbetta M, Van Essen DC, Raichle ME. 2005. The human brain is intrinsically organized into dynamic, anticorrelated functional networks. *Proc Natl Acad Sci U S A*. 102(27):9673–9678.

Fusar-Poli P, Placentino A, Carletti F, Landi P, Allen P, Surguladze S, Benedetti F, Abbamonte M, Gasparotti R, Barale F, et al. 2009. Functional atlas of emotional faces processing: a voxel-based meta-analysis of 105 functional magnetic resonance imaging studies. *J Psychiatry Neurosci*. 34(6):418–432.

Galan RF. 2008. On how network architecture determines the dominant patterns of spontaneous neural activity. *PLoS One*. 3(5).

Garrett DD, Kovacevic N, McIntosh AR, Grady CL. 2013. The modulation of bold variability between cognitive states varies by age and processing speed. *Cereb Cortex*. 23(3): 684–693.

Glasser MF, Sotiropoulos SN, Wilson JA, Coalson TS, Fischl B, Andersson JL, Xu J, Jbabdi S, Webster M, Polimeni JR, et al. 2013. The minimal preprocessing pipelines for the human connectome project. *Neuroimage*. 80:105–124.

Gu S, Pasqualetti F, Cieslak M, Telesford QK, Yu AB, Kahn AE, Medaglia JD, Vettel JM, Miller MB, Grafton ST, et al. 2015. Controllability of structural brain networks. *Nat Commun*. 6:8414.

Hagmann P, Cammoun L, Gigandet X, Meuli R, Honey CJ, Wedeen VJ, Sporns O. 2008. Mapping the structural core of human cerebral cortex. *PLoS Biol*. 6(7):e159.

Honey CJ, Sporns O, Cammoun L, Gigandet X, Thiran JP, Meuli R, Hagmann P. 2009. Predicting human resting-state functional connectivity from structural connectivity. *Proc Natl Acad Sci U S A*. 106(6):2035–2040.

Jeganathan J, Perry A, Bassett DS, Roberts G, Mitchell PB, Breakspear M. 2018. Fronto-limbic dysconnectivity leads to impaired brain network controllability in young people with bipolar disorder and those at high genetic risk. *Neuroimage Clin*. 19:71–81.

Kalman RE. 1963. Mathmatical description of linear dynamical systems. *SIAM Rev*. 5(2): 186.

Krishnan A, Williams LJ, McIntosh AR, Abdi H. 2011. Partial least squares (pls) methods for neuroimaging: a tutorial and review. *NeuroImage*. 56(2):455–475.

Lee WH, Frangou S. 2017a. Emergence of metastable dynamics in functional brain organization via spontaneous fmri signal and whole-brain computational modeling. *Conf Proc IEEE Eng Med Biol Soc*. 2017:4471–4474.

Lee WH, Frangou S. 2017b. Linking functional connectivity and dynamic properties of resting-state networks. *Sci Rep*. 7(1):16610.

Lindquist KA, Satpute AB, Wager TD, Weber J, Barrett LF. 2016. The brain basis of positive and negative affect: evidence from a meta-analysis of the human neuroimaging literature. *Cereb Cortex*. 26(5):1910–1922.

Lynn CW, Bassett DS. 2019. The physics of brain network structure, function and control. *Nat Rev Phys*. 1(5): 318–332.

McIntosh AR, Lobaugh NJ. 2004. Partial least squares analysis of neuroimaging data: applications and advances. *NeuroImage*. 23(Suppl 1):S250–S263.

Menon V, Uddin LQ. 2010. Saliency, switching, attention and control: a network model of insula function. *Brain Struct Funct*. 214(5–6):655–667.

Misic B, Sporns O. 2016. From regions to connections and networks: new bridges between brain and behavior. *Curr Opin Neurobiol*. 40:1–7.

Niendam TA, Laird AR, Ray KL, Dean YM, Glahn DC, Carter CS. 2012. Meta-analytic evidence for a superordinate cognitive control network subserving diverse executive functions. *Cogn Affect Behav Neurosci*. 12(2):241–268.

Pasqualetti F, Zampieri S, Bullo F. 2014. Controllability metrics, limitations and algorithms for complex networks. *IEEE Transactions on Control of Network Systems*. 1(1):40–52.

Pestilli F, Yeatman JD, Rokem A, Kay KN, Wandell BA. 2014. Evaluation and statistical inference for human connectomes. *Nat Methods*. 11(10):1058–1063.

Power JD, Cohen AL, Nelson SM, Wig GS, Barnes KA, Church JA, Vogel AC, Laumann TO, Miezin FM, Schlaggar BL, et al. 2011. Functional network organization of the human brain. *Neuron*. 72(4):665–678.

Raichle ME, MacLeod AM, Snyder AZ, Powers WJ, Gusnard DA, Shulman GL. 2001. A default mode of brain function. *Proc Natl Acad Sci U S A*. 98(2):676–682.

Roalf DR, Quarmley M, Elliott MA, Satterthwaite TD, Vandekar SN, Ruparel K, Gennatas ED, Calkins ME, Moore TM, Hopson R, et al. 2016. The impact of quality assurance assessment on diffusion tensor imaging outcomes in a large-scale population-based cohort. *NeuroImage*. 125:903–919.

Rubinov M, Sporns O. 2010. Complex network measures of brain connectivity: uses and interpretations. *NeuroImage*. 52(3):1059–1069.

Shrout PE, Fleiss JL. 1979. Intraclass correlations: uses in assessing rater reliability. *Psychol Bull*. 86(2):420–428.

Sinclair B, Hansell NK, Blokland GA, Martin NG, Thompson PM, Breakspear M, de Zubicaray GI, Wright MJ, McMahon KL. 2015. Heritability of the network architecture of intrinsic brain functional connectivity. *NeuroImage*. 121:243–252.

Smith SM, Fox PT, Miller KL, Glahn DC, Fox PM, Mackay CE, Filippini N, Watkins KE, Toro R, Laird AR, et al. 2009. Correspondence of the brain's functional architecture during activation and rest. *Proc Natl Acad Sci U S A*. 106(31): 13040–13045.

Sotiropoulos SN, Jbabdi S, Xu J, Andersson JL, Moeller S, Auerbach EJ, Glasser MF, Hernandez M, Sapiro G, Jenkinson M, et al. 2013. Advances in diffusion mri acquisition and processing in the human connectome project. *NeuroImage*. 80: 125–143.

Sporns O, Chialvo DR, Kaiser M, Hilgetag CC. 2004. Organization, development and function of complex brain networks. *Trends Cogn Sci*. 8(9):418–425.

Stiso J, Khambhati AN, Menara T, Kahn AE, Stein JM, Das SR, Gorniak R, Tracy J, Litt B, Davis KA, et al. 2018. White matter network architecture guides direct electrical stimulation through optimal state transitions. *ArXiv e-prints*. https://ui.adsabs.harvard.edu/#abs/2018arXiv180501260S (last accessed 1 May 2018).

Strike LT, Hansell NK, Couvy-Duchesne B, Thompson PM, de Zubicaray GI, McMahon KL, Wright MJ. 2018. Genetic complexity of cortical structure: differences in genetic and environmental factors influencing cortical surface area and thickness. *Cereb Cortex*.

Stuss DT, Alexander MP. 2000. Executive functions and the frontal lobes: a conceptual view. *Psychol Res*. 63(3–4): 289–298.

Tang E, Bassett DS. 2018. Colloquium: control of dynamics in brain networks. *Rev Mod Phys*. 90(3).

Tang E, Giusti C, Baum GL, Gu S, Pollock E, Kahn AE, Roalf DR, Moore TM, Ruparel K, Gur RC, et al. 2017. Developmental increases in white matter network controllability support a growing diversity of brain dynamics. *Nat Commun*. 8(1): 1252.

Thomas C, Ye FQ, Irfanoglu MO, Modi P, Saleem KS, Leopold DA, Pierpaoli C. 2014. Anatomical accuracy of brain connections derived from diffusion mri tractography is inherently limited. *Proc Natl Acad Sci U S A*. 111(46):16574–16579.

Tzourio-Mazoyer N, Landeau B, Papathanassiou D, Crivello F, Etard O, Delcroix N, Mazoyer B, Joliot M. 2002. Automated anatomical labeling of activations in spm using a macroscopic anatomical parcellation of the mni mri single-subject brain. *NeuroImage*. 15(1):273–289.

van den Heuvel MP, Sporns O. 2013. Network hubs in the human brain. *Trends Cogn Sci*. 17(12):683–696.

Van Essen DC, Ugurbil K, Auerbach E, Barch D, Behrens TE, Bucholz R, Chang A, Chen L, Corbetta M, Curtiss SW, et al. 2012. The human connectome project: a data acquisition perspective. *NeuroImage*. 62(4):2222–2231.

Ward JH. 1963. Hierarchical grouping to optimize an objective function. *J Am Stat Assoc*. 58(301): 236.

Wu-Yan E, BR F, Tang E, Gu S, Pasqualetti F, Bassett DS. 2018. Benchmarking measures of network controllability on canonical graph models. *J Nonlinear Sci*.

Yeh FC, Verstynen TD, Wang Y, Fernandez-Miranda JC, Tseng WY. 2013. Deterministic diffusion fiber tracking improved by quantitative anisotropy. *PLoS One*. 8(11):e80713.

Yeh FC, Wedeen VJ, Tseng WY. 2010. Generalized q-sampling imaging. *IEEE Trans Med Imaging*. 29(9):1626–1635.

Yeo BT, Krienen FM, Sepulcre J, Sabuncu MR, Lashkari D, Hollinshead M, Roffman JL, Smoller JW, Zollei L, Polimeni JR, et al. 2011. The organization of the human cerebral cortex estimated by intrinsic functional connectivity. *J Neurophysiol*. 106(3):1125–1165.

Zalesky A, Fornito A, Harding IH, Cocchi L, Yucel M, Pantelis C, Bullmore ET. 2010. Whole-brain anatomical networks: does the choice of nodes matter? *NeuroImage*. 50(3):970–983.

Zimmermann J, Griffiths JD, McIntosh AR. 2018. Unique mapping of structural and functional connectivity on cognition. *J Neurosci*. 38(45):9658–9667.